3D PHOTOACOUSTIC TOMOGRAPHY SETUP CALIBRATION

INDRAJEET MANIK TAMBE

A dissertation submitted for the partial fulfillment of BS-MS dual degree in Science

Indian Institute of Science Education and Research Mohali

April 2019

Certificate of Examination

This is to certify that the dissertation titled "3D PHOTO-ACOUSTIC TOMOGRAPHY SETUP CALIBRATION" submitted by Mr. Indrajeet Manik Tambe (Reg. No. M14186) for the partial fulfilment of BS-MS dual degree programme of the Institute, has been examined by the thesis committee duly appointed by the Institute. The committee finds the work done by the candidate satisfactory and recommends that the report be accepted.

Dr. Abhishek Chaudhuri Dr. Kamal P. Singh Dr. Samir K. Biswas

(Supervisor)

Dated: April 21,2019

Declaration

The work presented in this dissertation has been carried out by me under the guidance of Dr. S. K. Biswas at the Indian Institute of Science Education and Research Mohali.

This work has not been submitted in part or in full for a degree, at the Indian Institute of Science Education and Research Mohali. Whenever contributions of others are involved, every effort is made to indicate this clearly, with due acknowledgement of collaborative research and discussions. This thesis is a bonafide record of original work done by me and all sources listed within have been detailed in the bibliography.

Mr. Indrajeet Manik Tambe

(Candidate)

Dated: April 21,2019

In my capacity as the supervisor of the candidate's project work, I certify that the above statements by the candidate are true to the best of my knowledge.

Dr. S. K. Biswas

(Supervisor)

Acknowledgement

I am extremely indebted to Dr. Samir Kumar Biswas for his guidance and constant management as well as for providing necessary information and needful materials for the project. It would not have been possible without the kind support and help by him. I would also like thank members of Bio photonics lab members those who have helped me.

Mr. Indrajeet Manik Tambe

List of Figures

Notation

Symbol	Name
$\boldsymbol{T}$	Center of rotation
$\boldsymbol{c}$	speed of ultrasound of reference medium
$\boldsymbol{d}$	Spacing between two detector elements
$\boldsymbol{l}$	Length of the linear array
$\boldsymbol{r}$	Radius of the curved array
Φ	Rotation angle
$\boldsymbol{p_0}$	Initial pressure
$\boldsymbol{P_s}$	Position of the external photoacoustic point source
$\boldsymbol{P_{d,i}}$	Position of the i_{th} sensor element
$\boldsymbol{P_{s,k}}$	Position of the k_{th} source
$\boldsymbol{t_i}$	Observed time of flight
$\boldsymbol{s_i}$	Sensor that detected the measurement
$\boldsymbol{\gamma_i}$	Source number responsible for this measurement

Contents

Summary

The photoacoustic tomography is a technique used to display an image representation of a cross section through a human body using a phenomenon of photoacoustic effect. In this phenomenon, acoustic energy is generated when optical energy is provided to photoacoustic object. Using the generated acoustic signal it is possible to obtain the image of optical absorption distribution of the object. By adding point Photoacoustic source, which when illuminated with pulsed optical energy acts as a point ultrasound source. It allows simultaneous imaging of optical absorption distribution, speed of ultrasound sound distribution and acoustic attenuation distribution. The 3D Photoacoustic tomography setup gives collection of the 2D image representation of a cross section through an object at different projection angle. By further processing of this 2D image's, the 3D representation of the object can be obtained. In order to get the accurate 3D representation of the object calibration of the setup is necessary. The presented thesis work deals with the calibration of the 3D imaging photoacoustic tomography setup. The accuracy of the reconstructed image representation of the 3D object is determined by the accuracy of the calibration of the setup. The exact geometrical (or calibration) parameters need to be known because of many factors like, a) Sensors position offset which arrive during fabrication is unknown, b) Difficult to align the detectors straight and exactly parallel to z-axis. c) Difficult to fix the centre of rotation at pre-assigned co-ordinates. To get the parameters algorithm that is mentioned further were followed.

The thesis work is divided into four parts; the first part consists of Introduction about the concepts that are used in this work.

The second part consists of construction simulation based model, which includes photoacoustic source and detector array rotating at different projections in 3D Photoacoustic tomography setup. This simulation based model is constructed in order to get raw detector signal.

The third part consists of signal processing of pressure wave (acoustic signal), because the received detector signal has noise and some low amplitude measurements. It includes extracting the time of flight using template based approach and a procedure is prescribed for the same. It also includes classifying the time of flight and grouping

them using RANSAC(3) method to recognize the source from which it is coming from, identify the number of sources and Estimate the position of sensors(16).

The fourth part consists of estimating the speed of ultrasound and centre of rotation of the detectors array by first obtaining the initial guess and then the final estimate. Accuracy of calibration was also included in this part to find the uncertainty in the estimated parameters(16). In the last section of this part thesis is concluded.

Chapter 1

Introduction

1.1 Motivation

NIR (near-infrared) light has a reasonable penetration depth of 10 - 100 mm in soft tissue (1), which makes it less harmful than Gamma radiation which are the most dangerous form of ionizing radiation. Using the photoacoustic signal also avoids 'radiation sickness', which can occur in the case of gamma radiation. The combined property of Light (photo) and sound (acoustic) is the strength of photoacoustic tomography. The pulse of the laser light can be adjusted such that the acoustic wave generated by it is ultrasound. The contrast depends on the absorption of optical energy which is high as compared to ultrasound imaging (ultrasound is involved in the detection process only). The resolution is high as compared to pure optical pure optical tomography, as it depends on scattering during propagation in soft tissue (ultrasound low scattering). Hence it has advantages over both pure optical pure optical tomography and pure ultrasound imaging.

The photoacoustic tomography is a technique which gives an image without any piercing or tampering of the object. Due to the non-ionizing property of photoacoustic tomography, it can be safely used in medical diagnostics which are related to the micro-vascular systems.

1.2 The photoacoustic effect

The photo acoustic effect is the conversion of absorbed optical (or electromagnetic energy) to acoustic energy. This phenomenon occurs due to the thermoelastic property of the material(5; 6). Pulsed optical energy is required to observe this phenomenon. When the emission of optical energy is 'ON', the optical energy is absorbed by the material which causes heating of the material and subsequent thermal expansion gives rise to initial pressure (p_0) within the material. This initial pressure propagates in space with time (outward), when the laser exposure is 'OFF' and material tries to retain its shape. Another acoustic wave is generated by introducing another laser pulse and same is followed to generate several acoustic waves.

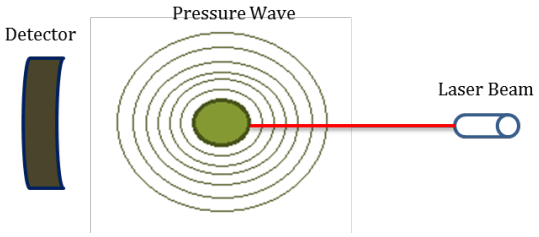

Figure (1.1) Photoacoustic effect

A short pulse of optical energy is required to generate an efficient or optimal pressure wave. The pulse width of the laser is determined by considering the conditions of thermal confinement and stress confinement. The heating of the material due to the absorption of optical energy can be represented with a space and time-dependent function H(r,t). This heating can be defined as the amount of absorbed energy per unit volume per unit time. If T(r,t) is the temperature distribution function then the resulting rise in temperature due to heating can be represented as (2):

$$\rho C_p \frac{\partial T(r,t)}{\partial t} = \lambda \nabla^2 T(r,t) + H(r,t) \tag{1.1}$$

ρ [kg/m^3] is the density of the material, C_p [J/(K kg)] is the specific heat and λ [J/(K m s)] is the thermal conductivity. Under the condition of thermal confinement heat diffusion can be neglected, so eq (1.1) will become:

$$\rho C_p \frac{\partial T(r,t)}{\partial t} \approx H(r,t) \tag{1.2}$$

Temperature rise in the confined volume is related to build up of local pressure. Due to the this pressure gradient the pressure wave propagates outwards which can be written as,

$$\boldsymbol{\nabla^2 p(r,t) - \frac{1}{c^2}\frac{\partial^2}{\partial t^2} p(r,t) = -\frac{\beta}{C_p}\frac{\partial}{\partial t} H(r,t)} \tag{1.3}$$

c [m/s] is the speed of ultrasound and $\boldsymbol{\beta[K^1]}$ is the volume thermal expansion coefficient.Now under the condition of thermal confinement, using (1.2), the generated excess acoustic pressure distribution is related to the heating function with a relation:

$$\boldsymbol{\nabla^2 p(r,t) - \frac{1}{c^2}\frac{\partial^2}{\partial t^2} p(r,t) = -\beta\rho\frac{\partial^2}{\partial t^2} T(r,t)} \tag{1.4}$$

The heating function can be written as purely spatial function A(r) representing the spatial distribution of the heat and a purely time dependent function $\boldsymbol{\delta}$(t) representing the time profile of the illuminating laser source. so H(r,t) = A(r) $\boldsymbol{\delta}$(t). The photo acoustic equation (equation 1.4) can be solved using Greens function approach and the final solution can be written as,

$$\boldsymbol{p(r,t) = \frac{\beta}{4\pi C_p}\frac{\partial}{\partial t}\left(\frac{1}{t}\iint_{||r'-r||=ct} A(r')d(r')\right)} \tag{1.5}$$

Initial pressure is at $\boldsymbol{t = o, p(r, t = 0)}$ is given by:

$$\boldsymbol{p_0(r) = \frac{\beta c^2}{C_p} A(r) = \Gamma A(r)} \tag{1.6}$$

Finally from equation (1.5) and (1.6) we get pressure equation(14; 15) in terms of initial pressure.

$$\boxed{\boldsymbol{p(r,t) = \frac{1}{4\pi c^2}\frac{\partial}{\partial t}\left\{\frac{1}{ct}\iint dr' p_0(r')\left(t - \frac{|r-r'|}{c}\right)\right\}}} \tag{1.7}$$

The above equation ignores acoustic attenuation and assumes that the speed

of sound is constant throughout the complete object. As attenuating effects requires a modified wave equation with a modified Green's function. The exact form of the time domain wave equation for acoustic attenuation, with its linear dependence on frequency as encountered in soft tissue, is still a big issue.

1.3 Measurement array geometries

There are three kinds of measurement arrays setup as presented in the following figure Figure 1.2, Figure 1.3 and Figure 1.4.

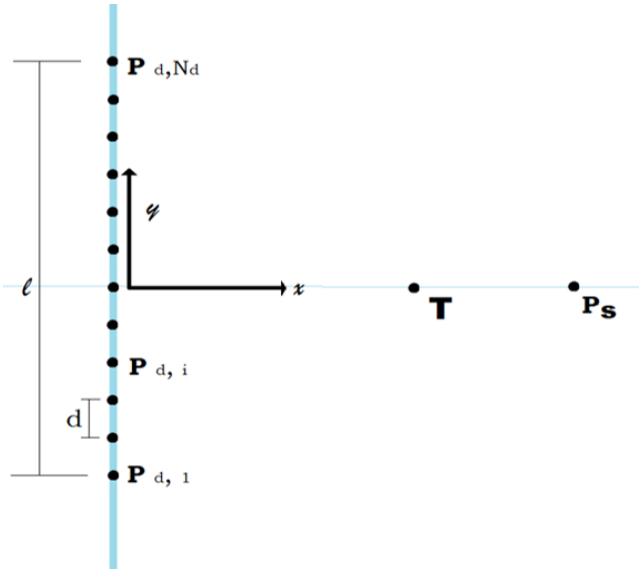

Figure (1.2) 2D linear detector array geometry

Figure 1.2 and Figure 1.3 are 2D models, where One consists of linear array(7; 8; 9; 10) with 128 detector elements and the other one consist of a curved array(11; 12; 13) with 32 detector elements. Figure 1.4 is a 3D model which is further used in this work.

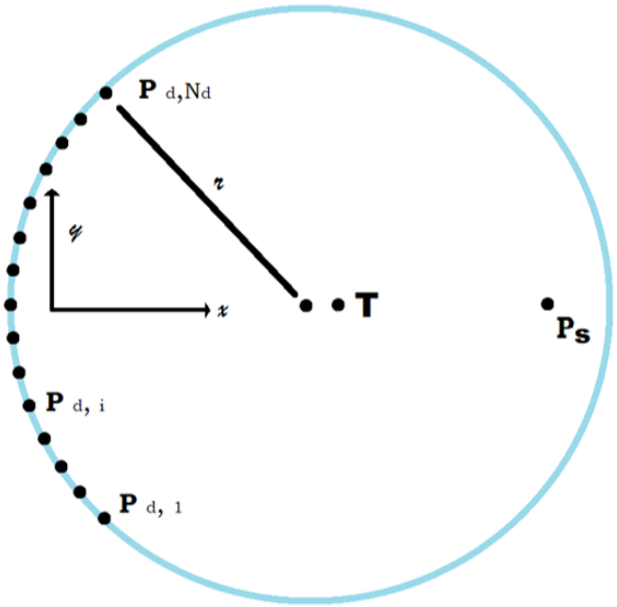

Figure (1.3) 2D curve detector array geometry

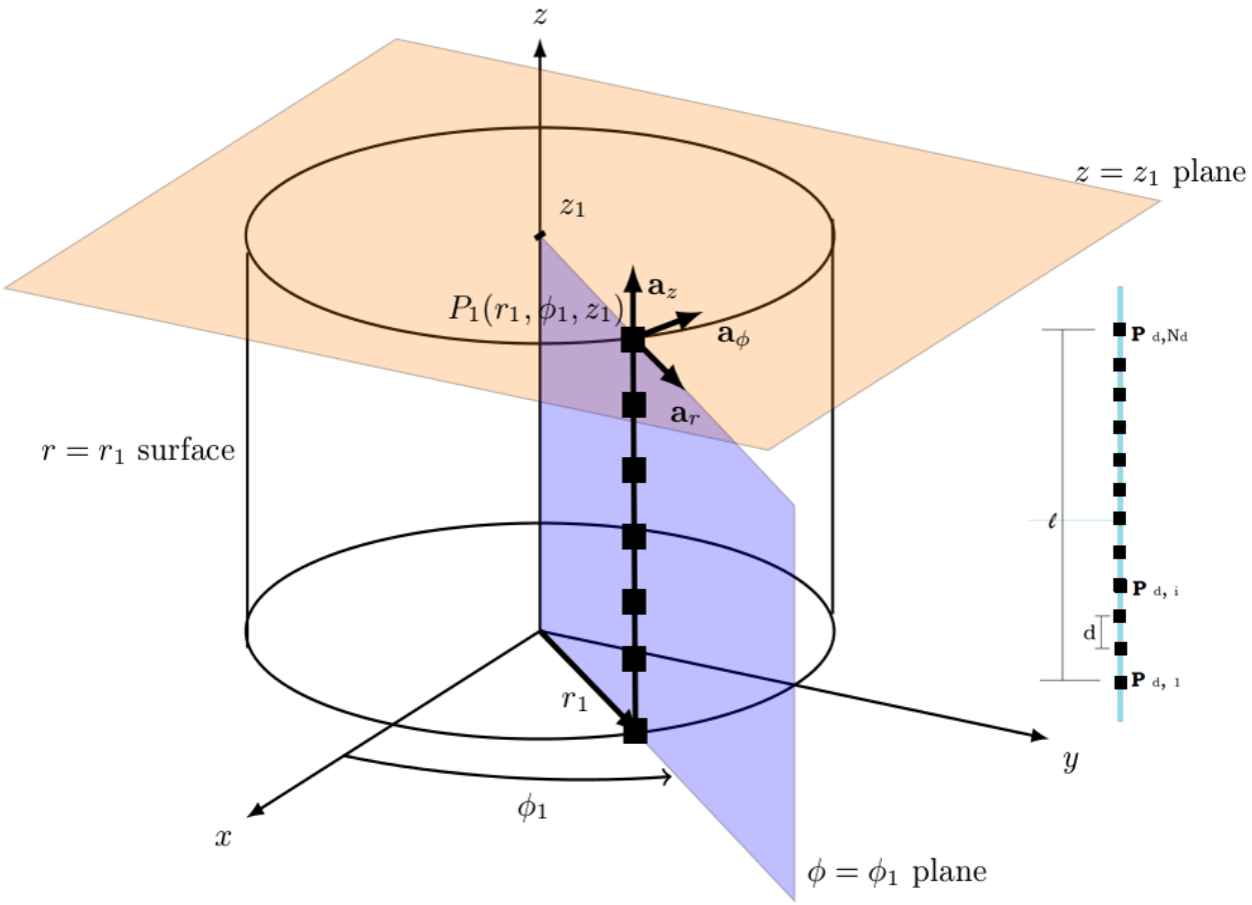

Figure (1.4) 3D Linear detector array along z-axis

The positions of the detector elements in all three geometries can be expressed in terms of the number of detector elements $\boldsymbol{N_d}$. Let us take the origin of the coordinate system as the middle of the measurement array, between two center elements. So the position of detectors in Figure 1.2 (curved array) can be given by:

$$\boldsymbol{P_{d,i}} = \boldsymbol{r} \begin{bmatrix} \boldsymbol{1 - cos\left\{\left(i - \frac{N_d+1}{2}\right)\frac{d}{r}\right\}} \\ \\ \boldsymbol{sin\left\{\left(i - \frac{N_d+1}{2}\right)\frac{d}{r}\right\}} \end{bmatrix}$$

The position of detectors in Figure 1.3 (linear array) can be deducted from curved array by letting the radius tend to infinity.

$$\boldsymbol{P_{d,i}} = \lim_{x\to\infty} \boldsymbol{r} \begin{bmatrix} \boldsymbol{1 - cos\left\{\left(i - \frac{N_d+1}{2}\right)\frac{d}{r}\right\}} \\ \\ \boldsymbol{sin\left\{\left(i - \frac{N_d+1}{2}\right)\frac{d}{r}\right\}} \end{bmatrix} = \begin{bmatrix} \boldsymbol{0} \\ \\ \boldsymbol{\left(i - \frac{N_d+1}{2}\right)d} \end{bmatrix}$$

The position of detectors for 3D model can be obtained using above two relation of position of detectors, with $\boldsymbol{\phi}$ as the rotation angle.

$$\boldsymbol{P_{d,i}} = \begin{bmatrix} \boldsymbol{rcos\Phi} \\ \\ \boldsymbol{rsin\Phi} \\ \\ \boldsymbol{\left(i - \frac{N_d+1}{2}\right)d} \end{bmatrix}$$

Before we proceed with the above-mentioned model, let's find what signal is received by a single detector from the source. 3D simulation based model having one detector, one source in 3D space are considered. (Figure 1.5 (d)). Figure 1.5 (a), Figure 1.5 (b) and Figure 1.5 (c) show propagating of the photoacoustic wave in the medium with time.

It's evident that the signal in Figure 1.5 (d) follows equation (1.7). In the next chapter, the above model is extended with 128 detector array arrangement in 3D as per geometry in Figure (1.3). This 128 detector array arrangement will produce a

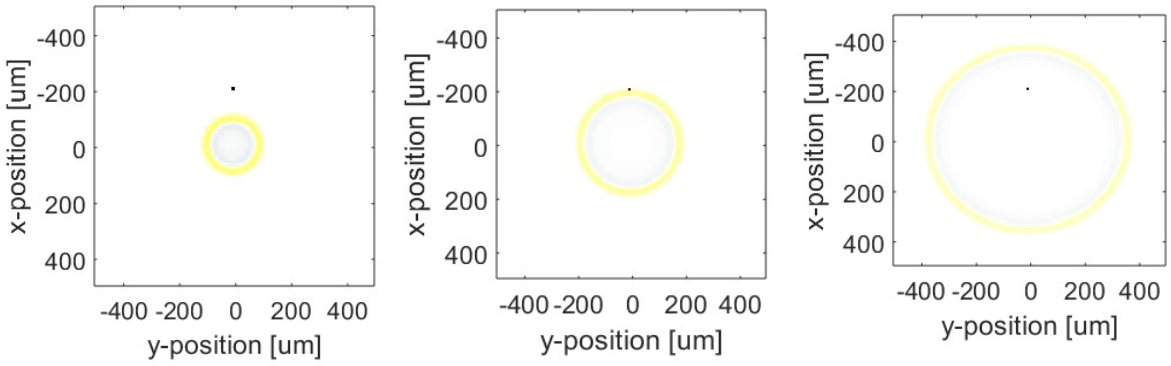

(a) (b) (c)

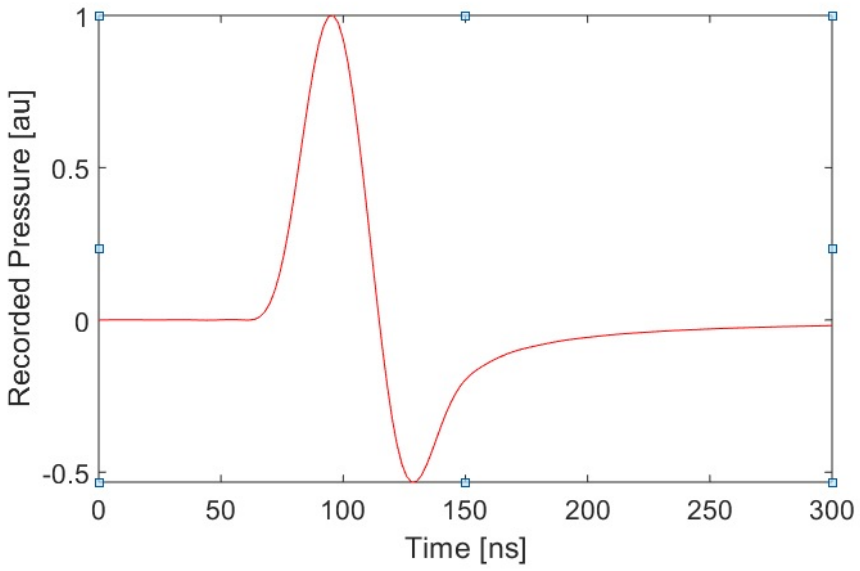

(d)

Figure (1.5) 2D model with 3 sources and 1 detector

similar type of signal with each detector. Processing or Analyzing this signal to find the geometrical parameters explained in further chapters.

Chapter 2

Model for calibration measurement

2.1 The calibration parameters

The geometrical parameters can be further bifurcated in terms of internal and external parameters. The internal parameters describe the measurement (detector) array. The external parameters describe the centre of rotation of the measurement setup, the speed of ultrasound of the reference medium and the positions of external photoacoustic point sources. Few parameters that we are interested in,

$\boldsymbol{T}$ - Center of rotation

$\boldsymbol{c}$ - speed of ultrasound of reference medium

$\boldsymbol{d}$ - Spacing between two detector elements

$\boldsymbol{l}$ - Length of the linear array

$\boldsymbol{r}$ - Radius of the curved array

$\boldsymbol{P_s}$ - Position of the external photoacoustic point source

$\boldsymbol{P_{d,i}}$ - Position of the $\boldsymbol{i_{th}}$ sensor element.

There will be one or more external point sources. The position of the external photoacoustic point source is crucial for the reconstruction of the acoustical properties; all alternative parameters are necessary for the reconstruction of both the acoustical as well as optical properties. We tend to assume that the internal parameters are fixed and do not change in between two measurement sessions and also assume that the external parameters are expected to change in between measurement sessions. However, remain is fixed during a single measurement session.

2.2 Construction of 3D Model

The setup for photoacoustic tomography in 3D was designed using 'k – wave' module in Matlab. In this simulation-based model point sources were constructed so as to generate the pressure wave. This pressure wave is similar to the pressure wave generated by the photoacoustic material when it is illuminated with a pulse laser. Another background condition's where included because the propagation in the simulation should be similar to the propagation in the practical medium. The point where propagating pressure is measured is considered as detector position as it is giving the same signal, that an ultrasound detector would give if placed in that same position. K – wave module does not have a specific ultrasound detector; hence we use a detector which detects the amplitude of the propagating pressure wave. It can be called as 'pseudo ultrasound detector'. Collection of such detectors are arranged in a linear array of 128 detectors (sensor array) as explained in chapter 1: Measurement array geometries section. The linear array was confined to a cylindrical path and placed at different projections (or at different angle **Φ** of the cylinder). The arrangement simulation model is shown in Figure (2.1) below, In the figure, the array is placed at five different projections, and the view from 2 different angles is demonstrated. The raw signal produced by this model is shown in Figure (2.2).

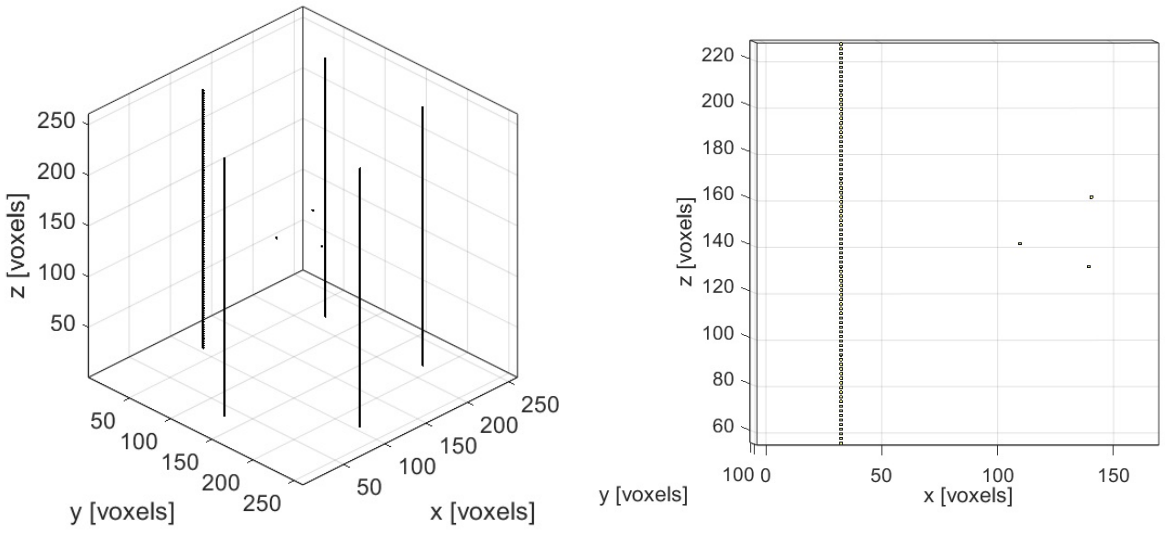

(a) (b)

Figure (2.1) 3D simulation model

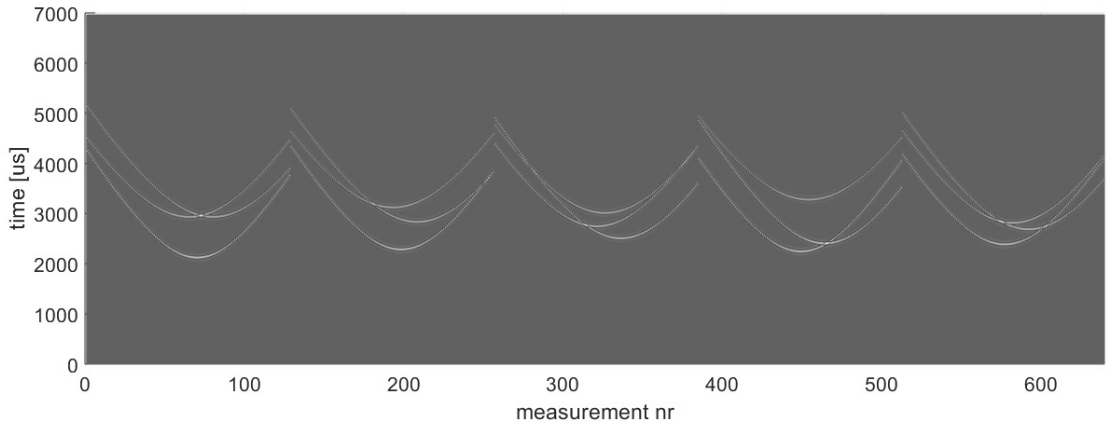

Figure (2.2)

Practically it very difficult to align the sensor array in a straight line parallel to z – axis. Sensors position offset which arrive during fabrication also need to be considered in the model. So purposeful inclination in z- axis was introduced in the model considering practical limitations. Figure (2.3) is the representation of a new model after considering the practical limitations and Figure (2.4) is its raw signal.

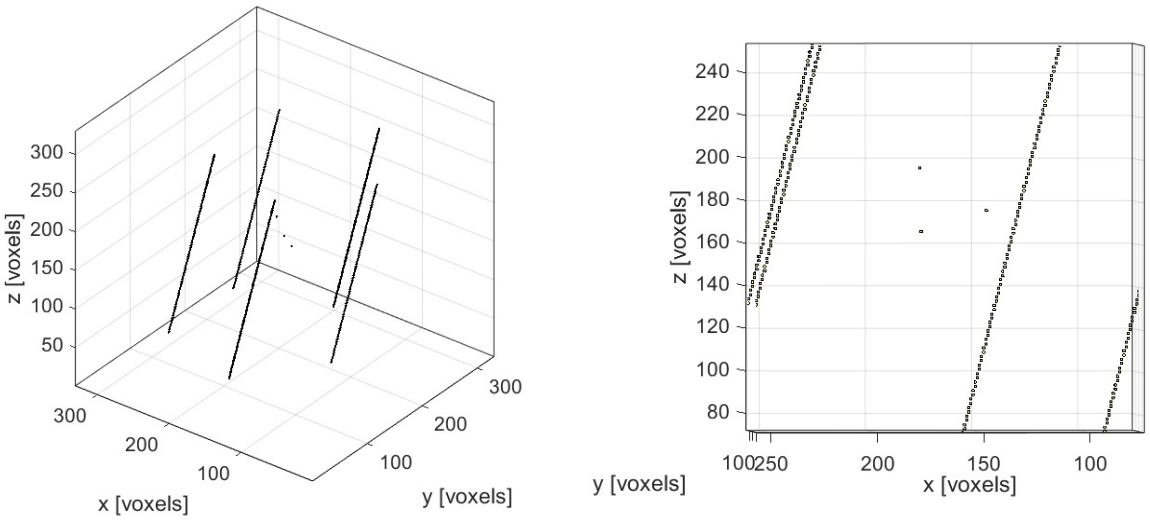

(a) (b)

Figure (2.3) 3D simulation model with practical correction

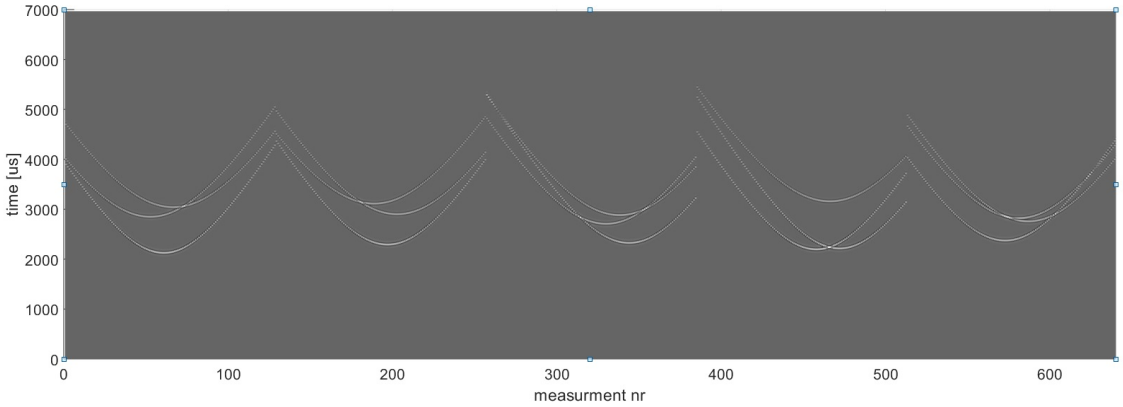
7000
6000
5000
4000
3000
2000
1000
0
time [us]
0
100
200
300
400
500
600
measurment nr

Figure (2.4)

Chapter 3

Calibration procedure

The necessary models and measurements required for calibration are introduced and analyzed; it's time to introduce the calibration procedure. The calibration procedure consists of many parts. First, we will prepossess the measured signals, resulting in the extraction of a set of time of flight measurements. Then a classification step is performed, which estimates the number of sources from the set of time of flight measurements and gives a classification of the measurements into groups identified by the source numbers. Once the measurements are classified to a group, we will introduce an approach to estimate the sensor positions and speed of ultrasound based on this classification result and the time of flight measurements. The calibration measurement requires an extra step so that all the measurements under different rotations are merged and finally result in the estimate of a speed of sound and centre of rotation.

3.1 Calibration phantom

In our model of the calibration measurement, we assumed that the speed of sound inside the calibration phantom and the speed of sound of the reference medium was equal. Practically, this might not be the case. Suppose that the speed of sound in the phantom is different than the speed of sound in the medium, but related to it via the relation $\boldsymbol{c_{phantom} = \alpha(c_{medium})}$. This is a valid relation when the phantom material

responds similarly to temperature fluctuations as the medium. Then the measurement function can be seen as to consist of two different parts, one part representing the ultrasound wave traveling through the reference medium and one representing the ultrasound wave traveling through the calibration phantom. The two different paths, let us consider the point $\boldsymbol{p_1}$ and $\boldsymbol{p_2}$, these are connected via the point $\boldsymbol{p_c}$ which lies on the boundary of the calibration phantom. The position of that point can be determined from the geometry of the phantom, the speed of sound of the phantom, the speed of sound of the medium, the position of the source $\boldsymbol{P_{s,k}}$ in the phantom, the position of the detector in the medium $\boldsymbol{p_d, i}$ and is governed by Snell's law. This results in a model that is related to the unknown parameters via the following equation (3.1). where $\boldsymbol{p_1}$ and $\boldsymbol{p_2}$ are the coordinates respectively of source position $\boldsymbol{k}$ and detector position $\boldsymbol{i}$ in the $\boldsymbol{j_{th}}$ rotation.

$$\boldsymbol{h_{tof,i,j,k}(c, T, P_{s,1}, ..., P_{s,N_p})} = \frac{\mathbf{1}}{\boldsymbol{c}}||\boldsymbol{p_2} - \boldsymbol{p_c}|| + \frac{\mathbf{1}}{\boldsymbol{ac}}||\boldsymbol{p_c} - \boldsymbol{p_1}|| \tag{3.1}$$

$$\boldsymbol{p_1} = \boldsymbol{R_{\phi j} p_{s,k}} \tag{3.2}$$

$$\boldsymbol{p_2} = \boldsymbol{p_{d,i}} - \boldsymbol{T} \tag{3.3}$$

3.2 Extracting time of flight measures

The most important step in the calibration procedure is the extraction of time of flight values from the measured signals. The measured signals contain a time-shifted and attenuated observation of the source signal in the presence of additive noise. The source signal is generated by a small optical absorber via the photoacoustic effect and the shape of this signal is primarily dependent on the size of the absorber. Because the measurement conditions and calibration phantom can change in between different measurement sessions, we might not know the exact source signal beforehand. Therefore, we seek a solution to the problem where we simultaneously try to estimate the time of flight values, the source signal and the attenuation factors from the measured

signals. A unique solution to this problem cannot be found because of the ambiguity in the phase and amplitude of the source signal with respect to the phases and amplitudes of the measurements. To overcome this problem, we will constrain the phase and amplitude of the source signal. The phase will be constrained by enforcing the centre of mass of the source signal to be exactly in the centre of the signal window. The mass coordinate will be the time, and the mass distribution will be the envelope of the source signal.

The amplitude of the source signal will be constrained by enforcing the maximum of the signal to be one. Now given a certain source signal, time of flight values and attenuation factors, it is straightforward to predict the measured signals. We aim to find the maximum likelihood estimate of all these unknown parameters from the observed measurements. In the presence of uncorrelated Gaussian noise with equal variance on all measurements, this results in searching for the least square error between the observed signals and predicted signals, subject to the two source signal constraints. The solution to this constrained least squares problem can be found in a simple iterative procedure, which has to be initialized with a rough guess of the source signal. The iterative solution is based on switching between solving for the time of flight and attenuation factors while keeping the source signal constant and solving for the source signal while keeping the time of flight and attenuation factors constant. In each iteration, after solving for the source signal, the constraints are applied to the source signal. The execution of the different steps is explained further.

3.2.1 STEP 1: Initialization for the source signal

A window in one of the source signal is considered such that it approximately covers the expected source signal as the signal may contain extra external noise.

3.2.2 STEP 2: Considering the source signal constraints

First the envelope of the source signal is calculated with the use of the Hilbert transform. The source signal is then shifted with the amount of mismatch between the calculated centre of mass and the centre of the signal window. This shifting is per-

formed using a Discrete Fourier transform (DFT) and an Inverse Discrete Fourier transform (IDFT) transform. Now the source signal is scaled by the inverse of its maximum so that the source signal is normalized to have a maximum value. After this step, the source signal obeys to the constraints.

3.2.3 STEP 3: Estimation of time of flight

As we have an estimate of the source signal, we can easily estimate the time of flight and attenuation factors. From the estimate of the source signal, a reference template is obtained, and after comparing this template with the actual, we get the time of flight measurement. Another approach is by taking distance the global maxima in each detector signal. More accuracy is attained by using a template-based approach.

3.2.4 STEP 4: Signal estimate

In this step, first all the measurement signal is shifted using the corresponding estimated time of flight value. Then the maximum likelihood estimate of the source signal is calculated using a weighted average of the shifted measured signals. The weighting factors are calculated based on the attenuation factors. From this step is a new estimate of the source signal, on which the constraints still have to be applied. So now after performing few iterations. Results converge to a stable solution, a local minimum to the non-linear least squares problem has been found.

3.2.5 STEP 5: Estimation of the source signal template

Using the envelope of each measured signal we identify possible source signals in the measured signals. When the envelope exceeds a certain threshold value, we extract a region of the measured signal around that position. On all the collected source signal realizations we perform the previously described time of flight/template estimation algorithm. This give's us an initial estimate of the source signal template which is used in the next step.

3.2.6 STEP 6: The Absolute time of flight measurement

With a given initial template estimate, we need to apply a filter match to the measured signals and find the local maxima in the resulting filtered signal. Now with this obtained local maxima we extract a part of the measured signal. On all the collected source signal realizations we perform the previously described time of flight/template estimation algorithm. The positions of the local maxima are taken into account to calculate the absolute time of flight within the whole measured signal.

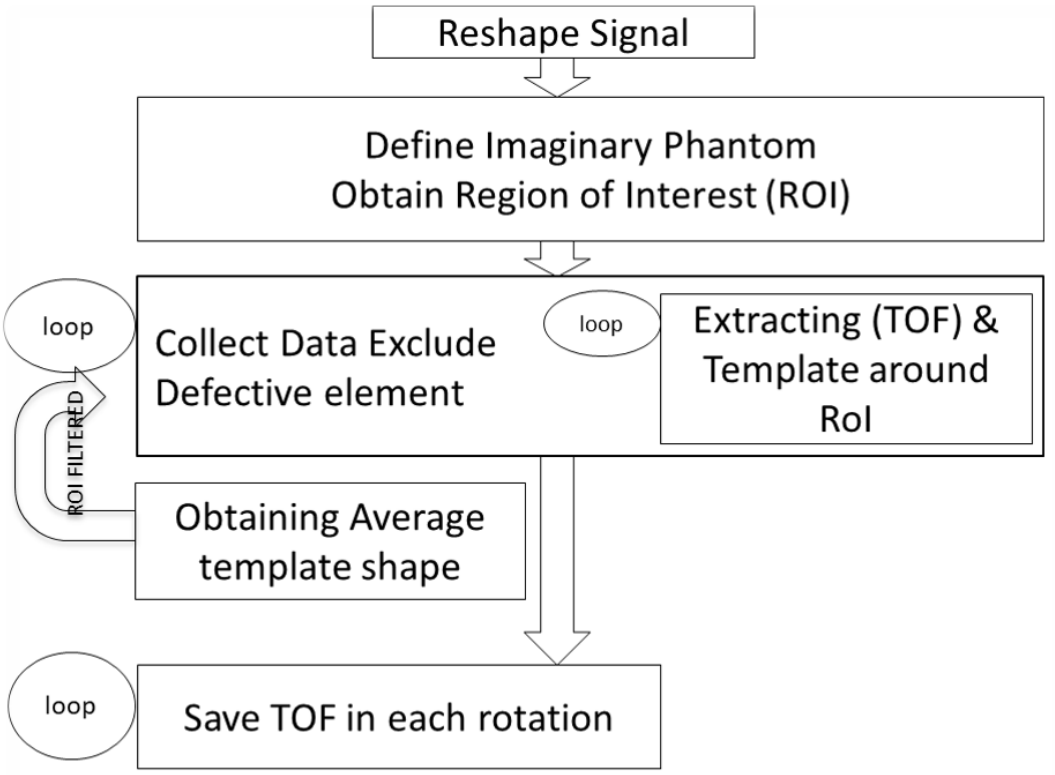

Figure (3.1) Time of flight Algorithm

After implementation of the above mention step and algorithm to process raw sensor data, the results in form if time of flight plot is exhibited in Figure (3.2). Five different partition represents the collection of sensor data at five different projection angle ($\mathbf{\Phi}$).

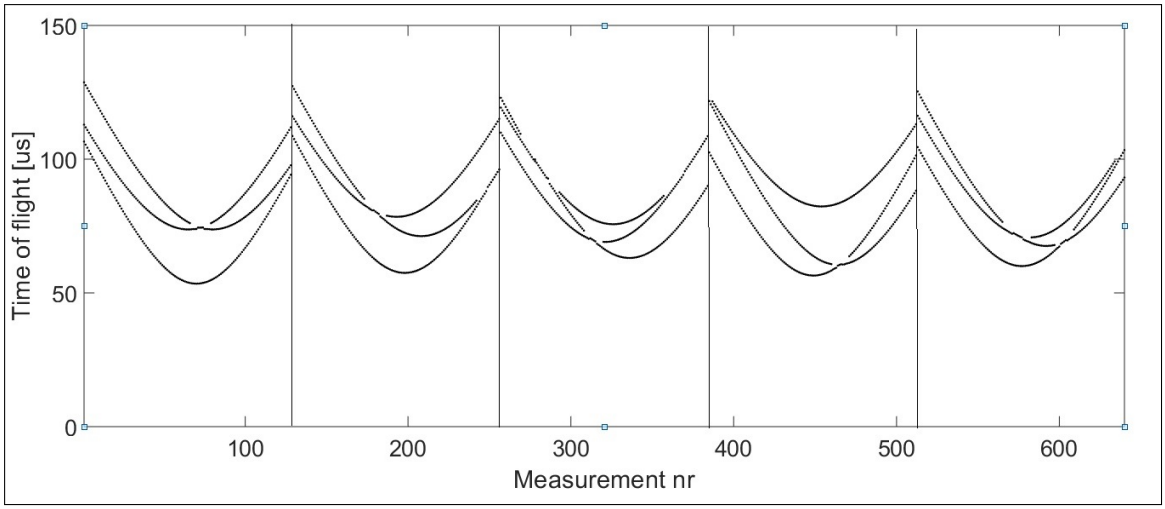

Figure (3.2) Time of flight Plot

From Figure (3.2) it can be concluded that the step contains more than one source (with no of curves of time of flight). When there are more than one source, it is expected that there could be outliers in the time of flight measurements. It is difficult to find the calibration parameters by directly fitting the (reference or calibration) model to the measurements. First, we need a classification step were the time of flight measurements are distinguished as being an outlier or belonging to either of the sources present in the measurement. The further section deals with the classification of time of flight measurements in different groups.

3.3 Grouping and maximum likelihood estimate

The procedure of our classification needs to be versatile so that it does not require the user to specify the number of sources beforehand but that it is estimated it from the measurements automatically. The classification procedure is carried out to determine the number of sources present in the measurements and to classify each of the time of flight measurements to one of the possible groups, where the possible groups are all of the sources plus an outlier group for false measurements (due to noise). The approach is based on using a mixture model to represent the measurements and then obtain a maximum likelihood estimate of the source parameters. In this procedure, we obtain the maximum likelihood estimate of the source parameters in each rotation separately. Because it is possible that not all sources are seen in every rotation. In

such a case source signal in the single rotation may overlap and may be seen that it belongs to the same group in likelihood estimate. The characteristic curve followed by the time of flight can be represented by a second-order polynomial. The deviation from this polynomial model can be considered as zero-mean Gaussian distributed with variance $\boldsymbol{\sigma_t^2}$.

Let us consider set of N time of flight measurements $\boldsymbol{t} = [\boldsymbol{t_1}, \boldsymbol{t_2}, .., \boldsymbol{t_N}]^{\boldsymbol{T}}$, if $\boldsymbol{s_i}$ is the sensor number of $\boldsymbol{i_{th}}$ measurement caused by the photoacoustic point source k and $\boldsymbol{x_k}$ is the polynomial parameters. The second order polynomial function that predicts the time of flight measurement at sensor $\boldsymbol{s_i}$ from the photoacoustic point source with polynomial parameters is given by the relation:

$$\boldsymbol{h_i(x_k) = x_{k,1} s_i^2 + x_{k,2} s_i + x_{k,3}} \tag{3.4}$$

A possible solution to the problem of finding the most likely set of second order polynomial functions describing the data can now be found maximizing this combined likelihood function. By this process, each measurement will be fully assigned to the group that is most likely. Sometimes there is a possibility that measurement might lie on the intersection of two polynomial curves, meaning that it could have originated quite well from either one of the two sources. Also, it might be a possibility that a measurement could equally well be an outlier or inlier. To identify the above situations, we need to first find the maximum likelihood estimate of $\boldsymbol{x}$, independent on $\boldsymbol{\gamma}$ and then find the probability that a certain measurement is the member of one of the groups. To find the likelihood function of $\boldsymbol{x}$, independent on $\boldsymbol{\gamma}$ we need to marginalize over the variable. From the existing information, we can calculate the probability of a particular measurement $\boldsymbol{t_i}$ belonging to group $\boldsymbol{\gamma_i}$ using the estimate of the most likely set of polynomial functions describing the data ($\boldsymbol{\Gamma}$).So the probability of all the inliers can obtained if $\boldsymbol{\gamma_i \geq 1}$, can be given as:

$$\boldsymbol{p(\gamma_i = k | t_i, \Gamma) = \frac{\exp\left(-\frac{1}{2}\frac{r_i^2(x_k)}{\sigma_t^2}\right)}{\sum_{k=1}^{N_s} \exp\left(-\frac{1}{2}\frac{r_i^2(x_k)}{\sigma_t^2}\right) + \frac{\sqrt{2\pi}\sigma_t}{v}}} \tag{3.5}$$

Similarly, the probability of all the outliers can obtained if $\boldsymbol{\gamma_i = 0}$ and can be given as:

$$p(\gamma_i = 0|t_i, \Gamma) = \frac{\frac{\sqrt{2\pi}\sigma_t^2}{w}}{\sum_{k=1}^{N_s} \exp\left(-\frac{1}{2}\frac{r_i^2(x_k)}{\sigma_t^2}\right) + \frac{\sqrt{2\pi}\sigma_t}{v}} \tag{3.6}$$

We need to maximize the above probability function for a correct estimate. So we will the global maximum and the number of groups based on RANSAC(3) mechanism. RANSAC is an algorithm which provides a proper fit for a mixture model that contains outliers. In this algorithm random sampling of whole set is done and are grouped into possible subsets in order to maximize the probability. For the given measurements parameter, residues to all measurements can be calculated with the following equation:

$$r_i(x) = h_i(x) - t \tag{3.7}$$

The process of Iteration is followed to increase N_s and data is distributed among different groups (= elements in N_s) such that there is no data left. After the classification of the last data point the iteration stops. The assign weight function will be dependent on the probability function and the residue element. The weight function can be given as:

$$w_{i,k}(\Gamma) = p(\gamma_i = k|t_i, \Gamma) = \frac{\exp\left(-\frac{1}{2}\frac{r_i^2(x_k)}{\sigma_t^2}\right)}{\sum_{k=1}^{N_s} \exp\left(-\frac{1}{2}\frac{r_i^2(x_k)}{\sigma_t^2}\right) + \frac{\sqrt{2\pi}\sigma_t}{v}} \tag{3.8}$$

$$w_{i,k}(\Gamma) = \begin{cases} 1, & \text{if } k = k_{min} \text{ and } \frac{r_i^2(x_k)}{\sigma_t^2} \leq f \\ 0, & \text{otherwise} \end{cases} \tag{3.9}$$

Where $f = -2log\ \frac{\sqrt{2\pi}\sigma_t}{v}$. RANSAC gives us random outcome. If $N_{S,min}$ is the minimum number of sources needed to find a fit to the model and N_{target} is the number of measurements we would like to be part of the new group. The probability of finding a solution after few trails is ϵ , we have the following relation:

$$N_{target,min} = \left\{ \frac{log(1-\epsilon)}{log\left(1 - \left(\frac{N_{target}}{N_o}\right)^{N_{s,min}}\right)} \right\} \tag{3.10}$$

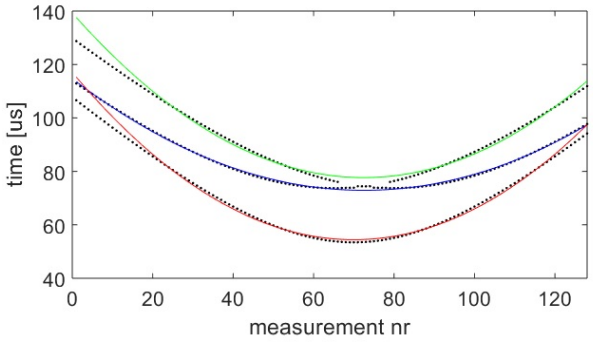

(a) $\phi = \mathbf{0^0}$

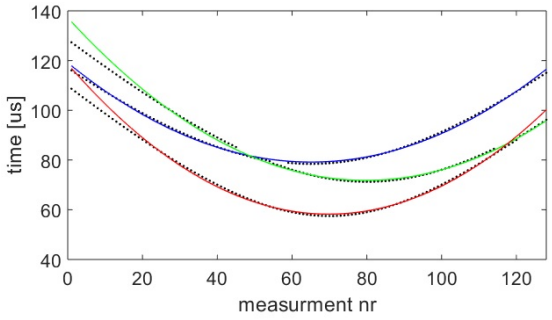

(b) $\phi = \mathbf{72^0}$

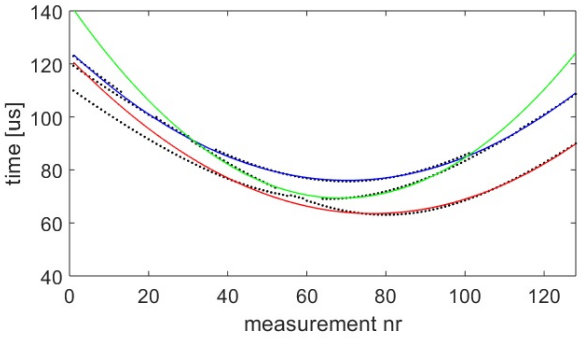

(c) $\phi = \mathbf{144^0}$

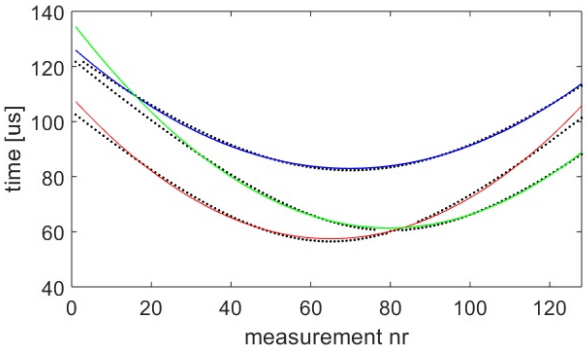

(d) $\phi = \mathbf{144^0}$

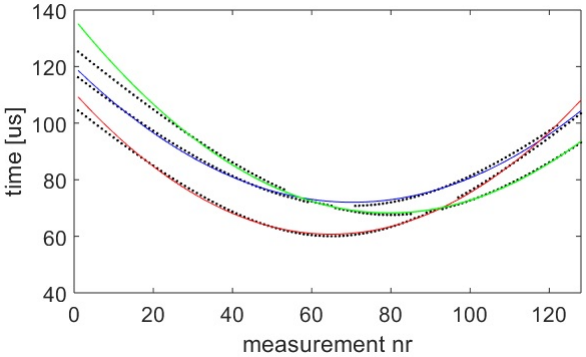

(e) $\phi = \mathbf{288^0}$

Figure (3.3) Grouping of time of flight measurments

In our setup we have $\boldsymbol{N_{s,min}}$, s = (a1, a2, a3), so the model fit is done with

the following equation:

$$\boldsymbol{x = H_s^{-1}\ z_s\ where\ H_s^{-1} = \begin{bmatrix} s_{a1}^2 & s_{a1} & 1 \\ s_{a2}^2 & s_{a2} & 1 \\ s_{a3}^2 & s_{a3} & 1 \end{bmatrix}} \tag{3.11}$$

Figure (3.3) shows the results of the Grouping of the time of flight measurements in 5 different projections. In the figure, the blue dots are the time of flight measurements, and the coloured solid line represents the fit of different group. The points which lie on or near the colour line are considered as one class or group. Here the final result obtained is number of source in each rotation.

Chapter 4

Center of rotation

In the previous chapter, we have extracted the time of flight measurement and grouped them to find number of sources. Using the parameters that we obtained we will proceed to find the speed of ultrasound and the center of rotation.

4.1 Estimate for speed of sound and source position

To find the speed of ultrasound ($\boldsymbol{c}$) and source position ($\boldsymbol{P_{s,k}}$) estimate, we will again look for the likelihood function of c and p with known measurements. We will use the maximum of this likelihood function as the estimate of $\boldsymbol{c}$ and $\boldsymbol{p}$. This likelihood function is similar to the likelihood function used in the previous chapter; the only difference is that rather than using the residues of the polynomial function parameter we use residues of the measurement function parameters $\boldsymbol{c}$ and $\boldsymbol{p}$. The likelihood function of c and p with measurements $\boldsymbol{t_i}$ is similar to Equation (3.12) and obtained in a similar way as Equation (3.12) in chapter 3.

$$\boldsymbol{p(t_i|c,p)} = \frac{\mathbf{1}}{\boldsymbol{(N_s+1)\sqrt{2\pi}\sigma_t}} \left(\sum_{\boldsymbol{k=1}}^{\boldsymbol{N_s}} \mathbf{exp} \left(-\frac{\mathbf{1}}{\mathbf{2}} \frac{\boldsymbol{r_i^2(c,p_{s,k})}}{\boldsymbol{\sigma_t^2}} + \frac{\boldsymbol{\sqrt{2\pi}\sigma_t}}{\boldsymbol{v}} \right) \right) \quad (4.1)$$

Similarly, the weighting function, in this case, can be deducted from Equation (3.18), it is given as:

$$\boldsymbol{w_{i,k}(c,p)} = \frac{\exp\left(-\frac{1}{2}\frac{r_i^2(c,p_{s,k})}{\sigma_t^2}\right)}{\sum_{k=1}^{N_s}\exp\left(-\frac{1}{2}\frac{r_i^2(c,p_{s,k})}{\sigma_t^2}\right) + \frac{\sqrt{2\pi}\sigma_t}{v}} \tag{4.2}$$

Now to find the weighted non-linear least square fit Gauss-Newton method(4) is used. In order to proceed further, we need to calculate the Jacobian matrix of the function of the residue vector. The Jacobian matrix of this function $\boldsymbol{r(x)}$ for a given estimate $\boldsymbol{x^{(l)}}$, where $\boldsymbol{l}$ is the iteration number of the Gauss-Newton method(4) can be given as follows:

$$\boldsymbol{H_{c,k}^{(l)}} = \begin{bmatrix} \frac{\partial}{\partial c}\boldsymbol{h_{1,k}^{(l)}}\sqrt{\boldsymbol{w_{1,k}}} \\ \vdots \\ \frac{\partial}{\partial c}\boldsymbol{h_{N,k}^{(l)}}\sqrt{\boldsymbol{w_{N,k}}} \end{bmatrix} \tag{4.3}$$

$$\boldsymbol{H_{p_k}^{(l)}} = \begin{bmatrix} \frac{\partial}{\partial p_{s,k}}\boldsymbol{h_{1,k}^{(l)}}\sqrt{\boldsymbol{w_{1,k}}} \\ \vdots \\ \frac{\partial}{\partial p_{s,k}}\boldsymbol{h_{N,k}^{(l)}}\sqrt{\boldsymbol{w_{N,k}}} \end{bmatrix} \tag{4.4}$$

$$\boldsymbol{H^{(l)}} = \begin{bmatrix} \boldsymbol{H_{c,1}^{(l)}} & \boldsymbol{H_{p_1}^{(l)}} & \\ \vdots & \ddots & \\ \boldsymbol{H_{c,N_s}^{(l)}} & & \boldsymbol{H_{p,N_s}^{(l)}} \end{bmatrix} \tag{4.5}$$

The no.of iterations by Gauss Newton method(4) required to optimize the complete parameter vector x in the given iteration is given as:

$$\boldsymbol{x^{(l+1)}} = \boldsymbol{x^{(l)}} - \boldsymbol{(H^{(l)T}H^{(l)})^{-1}H^{(l)T}\ r(x^{(l)})} \tag{4.6}$$

The no. of iterations by Gauss Newton method(4) required to optimize the source position in the given iteration with initial guess of speed of ultrasound $\boldsymbol{c = 1500 m/s}$ is given as: Using the above iterations the data could obtain apparent source. It does not represent a physical source as it is the set of measurements that can be well described with a polynomial function.

$$\boldsymbol{p_{s,k}^{(l+1)} = p_{s,k}^{(l)} - (H_{p_k}^{(l)T} H_k^{(l)})^{-1} H_k^{(l)T}\ r(p_{s,k}(l))} \tag{4.7}$$

4.2 Estimation of Source Position and Centre of rotation

In the previous section, we have obtained a set of the speed of ultrasound and relative source positions in each rotation. Now we find the initial guess of the centre of rotation and source position on the estimates of the previous step. Finally, this initial guess will be used in the optimization step to find the complete likelihood function. We select a pair of relative source position in different rotations estimated in the previous section. The relative source position, the absolute source position and the center of rotation are related to each other by the following relation, given as:

$$\boldsymbol{p'_{s,k_1} = R_{\phi R_1}\ p_{s,k} + T} \tag{4.8}$$

$$\boldsymbol{p'_{s,k_2} = R_{\phi R_2}\ p_{s,k} + T} \tag{4.9}$$

where,

$$\boldsymbol{R_\phi} = \begin{bmatrix} \boldsymbol{cos\phi} & \boldsymbol{-sin\phi} & \boldsymbol{0} \\ \boldsymbol{sin\phi} & \boldsymbol{cos\phi} & \boldsymbol{0} \\ \boldsymbol{0} & \boldsymbol{0} & \boldsymbol{1} \end{bmatrix} \tag{4.10}$$

combining Equation (4.8) and (4.9), we get:

$$\begin{bmatrix} \boldsymbol{p'_{s,k_1}} \\ \boldsymbol{p'_{s,k_2}} \end{bmatrix} = \boldsymbol{A} \begin{bmatrix} \boldsymbol{p_{s,k}} \\ \boldsymbol{T} \end{bmatrix} \text{ where, } \boldsymbol{A} = \begin{bmatrix} \boldsymbol{R_{\phi R_1}} & \boldsymbol{I} \\ \boldsymbol{R_{\phi R_2}} & \boldsymbol{I} \end{bmatrix}$$

So, from Equation (4.11) we get the absolute source position and center of rotation. A is be 6 x 6 matrix in our case, and the final matrix that we get is 6 x 3 in this matrix top 3 x 3 element's represents absolute source position and lower half of 3 x 3 represents T. In the further section we look for the uncertainty on the estimates of both the parameters.

$$\begin{bmatrix} \boldsymbol{p_{s,k}} \\ \boldsymbol{T} \end{bmatrix} = \boldsymbol{A^{-1}} \begin{bmatrix} \boldsymbol{p'_{s,k_1}} \\ \boldsymbol{p'_{s,k_2}} \end{bmatrix} \tag{4.11}$$

4.3 Accuracy of calibration

To get an idea of uncertainty in the estimated parameters(16), We need to find the elements of co-variance matrix. Similarly to Equation (4.6) we have a relation for number of iteration for Gauss-Newtons method(4) can be given as:

$$\boldsymbol{x^{(l+1)}} = \boldsymbol{b^{(l)}} - (\boldsymbol{H^{(l)T}} \boldsymbol{H^{(l)}})^{-1} \boldsymbol{H^{(l)T}}\ \boldsymbol{r(x^{(l)})} = \boldsymbol{b^{(l)}} + \boldsymbol{At'} \tag{4.12}$$

Where $\boldsymbol{t'}$ is related to weighted measurements with relation $\boldsymbol{t'} = \boldsymbol{Wt}$ and the weight matrix can be given as:

$$\boldsymbol{W} = \begin{bmatrix} \boldsymbol{diag}(\sqrt{\boldsymbol{w_{1,1}}}, ..., \sqrt{\boldsymbol{w_{N,1}}}) \\ \vdots \\ \boldsymbol{diag}(\sqrt{\boldsymbol{w_{1,N_s}}}, ..., \sqrt{\boldsymbol{w_{N,N_s}}}) \end{bmatrix} \tag{4.13}$$

Now we perform linear transformation of the measurements with known co-variance matrix $\boldsymbol{P_{tt}} = \boldsymbol{I\sigma_t^2}$. So finally we get the co-variance matrix of the estimated

parameters and is given by the following relation:

$$\boldsymbol{P_{AA} = AWP_{tt}W^TA^T = AWW^TA^T\sigma_w^2} \tag{4.14}$$

4.4 Conclusion

The setup of 3-D photoacoustic tomography can be calibrated with the help received detector signal. The algorithm provides an estimate of calibration parameters using time of flight measurements. Increase in number. of detectors may lead to an increase in the accuracy of calibration parameters. An initial guess is required to begin the iteration process of the algorithm. The algorithm automatically detects the number. of sources and the amount of noise. It also consists calculation for accuracy of calibration, where the accuracy is checked and if required accuracy is not met it estimates the parameters again. Using the photoacoustic model eliminates the limitations of the pure ultrasound model and the pure optical model for image reconstruction. This algorithm can simultaneously run with the algorithm of image reconstruction so that if the center of rotation changes due to instrumental error detects the change and hence will not reduce the image quality.

Bibliography

[1] L. V. Wang and H. I. Wu, *Biomedical Optics: principles and imaging.* WileyInterscience, 2007.

[2] R. A. Kruger, P. Liu, Y. R. Fang, and C. R. Appledorn, *"Photoacoustic ultrasound (PAUS)–reconstruction tomography,"* Med. Phys., vol. 22, no. 10, pp. 1605–1609, 1995.

[3] M. A. Fischler and R. C. Bolles, *"Random sample consensus: a paradigm for model fitting with applications to image analysis and automated cartography,"* Commun. ACM, vol. 24, no. 6, pp. 381–395, 1981.

[4] R. Fletcher, *Practical methods of optimization.* John Wiley, 1987.

[5] M. W. Sigrist and F. K. Kneubhl, *"Laser-generated stress waves in liquids,"* J. Acoust. Soc. Am., vol. 64, pp. 1652–1663, 1978.

[6] G. Paltauf and P. E. Dyer, *"Photomechanical processes and effects in ablation,"* Chem. Rev., vol. 103, pp. 487–518, 2003.

[7] R. G. M. Kolkman, P. J. Brands, W. Steenbergen, and T. G. van Leeuwen, *"Real-time in vivo photoacoustic and ultrasound imaging,"* Journal of Biomedical Optics, vol. 13, no. 5, p. 050510, 2008.

[8] R. J. Zemp, R. Bitton, M.-L. Li, K. K. Shung, G. Stoica, and L. V. Wang, *"Photoacoustic imaging of the microvasculature with a high-frequency ultrasound array transducer,"* Journal of Biomedical Optics, vol. 12, no. 1, p. 010501, 2007.

[9] J. J. Niederhauser, M. Jaeger, R. Lemor, P. Weber, and M. Frenz, *"Combined ultrasound and optoacoustic system for real-time high-contrast vascular imaging in vivo,"* IEEE Trans Med Imaging, vol. 24, p. 436440, 2005.

[10] Y. Zeng, D. Xing, Y. Wang, B. Yin, and Q. Chen, *"Photoacoustic and ultrasonic coimage with a linear transducer array,"* Opt. Lett., vol. 29, no. 15, pp. 1760–1762, 2004.

[11] R. A. Kruger, D. R. Reinecke, and G. A. Kruger, *"Thermoacoustic computed tomography – technical consideration,"* Med. Phys., vol. 26, pp. 1832 – 1837, 1999

[12] X. Wang, Y. Pang, G. Ku, X. Xie, G. Stoica, and L.-H. Wang, *"Noninvasive laserinduced photoacoustic tomography for structural and functional in vivo imaging of the brain,"* Nature Biotech, vol. 21, p. 803, 2003.

[13] R. Ma, A. Taruttis, V. Ntziachristos, and D. Razansky, *"Multispectral optoacoustic tomography (msot) scanner for whole-body small animal imaging,"* Opt. Express, vol. 17, pp. 21414–21426, 2009.

[14] Lihong V. Wang (invited paper) *"Tutorial on Photo acoustic Microscopy and Computed Tomography"*

[15] S.K. Biswas, P. van Es, W. Steenbergen, R. M. Vasu, S. Manohar, paper *"Regularization free non- symmetric model matrix based iterative photo acoustic image".*

[16] Rene Willemink, University of Twente Research Thesis *"IMAGE RECONSTRUCTION IN A PASSIVE ELEMENT ENRICHED PHOTOACOUSTIC TOMOGRAPHY SETUP"*

[17] P. van Es, S. K. Biswas, H. J. B. Moens, W. Steenbergen, S. Manohar, *"Initial results of finger imaging using photoacoustic computed tomography"* Journal of biomedical optics, vol. 19 no. 6, p. 060501, 2014.

[18] S. K. Biswas, P. van Es, W. Steenbergen, S. Manohar, *"A method for delineation of bone surfaces in photoacoustic computed tomography of the finger"* Journal of Applied Physics, vol. 38 no. 1, p. 63-76, 2016

[19] P. van Es, S. K. Biswas, H. J. B. Moens, W. Steenbergen, S. Manohar, *"Photoacoustic tomography of the human finger: towards the assessment of inflammatory joint diseases"* Photons Plus Ultrasound: Imaging and Sensing 9323, pp. 93234Q, 2015

[20] S. K. Biswas, P. van Es, W. Steenbergen, S. Manohar, *"A new approach to depict bone surfaces in finger imaging using photoacoustic tomography"* Photons Plus Ultrasound: Imaging and Sensing 9323, pp. 932322, 2015

[21] P. van Es, S. K. Biswas, B. H. J. Moens, W. Steenbergen, S. Manohar, *"Hunting the synovium in Rheumatoid Arthritis: photoacoustic finger joint imaging"*